SUPPLEMENTARY INFORMATION

Sample preparations

$Fe_{0.5}Co_{0.5}Si$ single crystal was grown by the floating zone technique. The phase purity and cation concentrations were checked by powder X-ray diffraction and Energy Dispersive X-ray spectroscopy (EDX), respectively. Bulk properties of the crystal were confirmed to be identical with those reported in literature[1]. Electron-transparent thin plate with thickness of about 20 nm was prepared by mechanical polishing and subsequent argon-ion thinning with an acceleration voltage of 4 kV at low temperatures.

Lorentz TEM microscopy and quantitative evaluation of Skyrmion crystal in $Fe_{0.5}Co_{0.5}Si$

The schematic of Lorentz transmission electron microscopy (TEM) is illustrated in the supplemental Fig. 1. When the electron beam was irradiated to a ferromagnet, Lorentz force induced by the magnetic components normal to the incident beam, should deflect the electron beam, resulting in the convergence/divergence images of magnetic domain walls at defocused image plane[2]. In this study, we changed the objective lens current to obtain the various magnetic fields along the z-axis, which were applied to thin plate $Fe_{0.5}Co_{0.5}Si$. Moreover, quantitative evaluation of Skyrmion structure, i.e., a lateral magnetization distribution map in Skyrmion crystal was achieved by using QPt[3], where three Lorentz micrographs (under-, in- and over-focused images) were analyzed using the transport-of-intensity equation (TIE Eq.) [4-5]

$$\frac{2\pi}{\lambda}\frac{\partial I(xyz)}{\partial z} = \nabla_{xy}\left[I(xyz)\nabla_{xy}\phi(xyz)\right], \tag{1}$$

that was derived from Schrödinger equation under the small angle approximation when the optical wave propagates through a phase object[4]. $I(xyz)$ and $\phi(xyz)$ stand for the

intensity and phase distributions of propagating optical wave, respectively. TIE Eq. was recently applied to the simulation for TEM observation of the thin plate[5], which can be also viewed as a weak phase object. On the other hand, according to the Maxwell-Ampére equations, in a magnetic field, $\phi(xyz)$ and the magnetization $\vec{M}$ has a relation as

$$\nabla_{xy}\phi(xyz) = -\frac{e}{\hbar}(\vec{M} \times \vec{n})t \,, \qquad (2)$$

where t is the thickness of the thin-plate sample, $\vec{n}$ the unit vector parallel to the beam direction. In order to find the magnetization ($\vec{M}$) distribution in x-y plane, we obtained $\frac{\partial I(xyz)}{\partial z}$, the change of electron intensity along z-axis, by analyzing the Lorentz microscopic images. Then by substituting $\frac{\partial I(xyz)}{\partial z}$ into Eq. (1), we obtained $\phi(xyz)$. Finally, we substituted $\phi(xyz)$ into Eq. (2) and found $\vec{M}$.

To get $\frac{\partial I(xyz)}{\partial z}$ from the experimental data, we expressed $\frac{\partial I(xyz)}{\partial z}$ approximately as

$$\frac{\partial I}{\partial z} \approx \frac{I(x, y, z_0 + \Delta z) - I(x, y, z_0 - \Delta z)}{2\Delta z} \,, \qquad (3)$$

where $2\Delta z$ is the distance of the over-focused and under-focused planes and $\Delta z \ll z_0$, with z_0 the focus distance of the objective lens. Since the electrostatic potential is a function of sample thickness, although it is much smaller than the high electron energy and the sample is thin enough, it should increase the noises in the phase distribution image. To get a good estimation of the phase distribution, TEM observation was carried out below the upper limit of the defocus distance which depends on the experimental condition and the initial magnetic property of the thin plate.

Supplemental Fig. 2 (a-c) shows three Lorentz micrographs under a magnetic field applied normal to the thin plate sample. The Skyrmion lattice was observed in the defocused images (Figs. 2a and 2b). The contrast is inversed in those two images, indicating a change in the electron intensity between under- and over-focused image planes. The magnetization distribution was obtained by the afore-mentioned TIE method and is shown in supplemental Fig. 2d. Such a TIE image demonstrates that the magnetic components in each spin "particle" are perpendicular to the external magnetic field expect for the core and the peripheral region of "particle", where the magnetic component is parallel to the field. In the array of such hexagonal spin "particles", namely Skyrmions, magnetic defects (indicated by yellow arrows) also exist. The possible origin of such defects may come from the layered disorder of Skyrmion.

Comparing the Skyrmion structures of the (001) plane with those of (110) plane (see supplemental Fig. 3), we find that two-dimensional Skyrmion density, evaluated as Skyrmion number[6], is higher on the (001) plane. We attribute this to the fact that more Skyrmion crystal defects have developed in the (110) plane.

Supplemental Fig. 4 represents the formation of Skyrmion crystal under a perpendicular magnetic field. A systematic investigation of the magnetic field dependence of the Skyrmion crystal structure reveals that multi-domains were created in the ordered Skyrmion crystal around the dislocations of underlying helical structure (indicated by white arrows in supplemental Fig. 3a). It was found that the Skyrmions start to emerge around such dislocations when increasing the magnetic field up to 20 mT. The coexistence of helical structure and Skyrmion lattice was also observed in the range of magnetic field from 20 mT to 40 mT. By further increasing the magnetic field to 50 mT, Skyrmion crystals are generated and the stripy structure is completely replaced. However, as displayed in supplemental Figs. 3d and 3e, multi-domains and domain

boundaries are also observable. Interestingly, the locations of the domain boundaries almost coincide with the afore-mentioned dislocations. In such Skyrmion crystal multi-domains, as marked by color hexagons, the hexagonal lattices of the single domains are also seen to rotate slightly from each other. Furthermore, as the applied magnetic field is high enough above 70 mT, the Skyrmion density decreases, accompanied by the increase of ferromagnetic domain. Accordingly, we conclude that a dislocation in a proper screw structure assists the formation of Skyrmion crystals but builds multi-domains in them.

Monte Carlo (MC) simulation

Spin interactions in $Fe_{0.5}Co_{0.5}Si$ can be modeled by the following three-dimensional (3D) lattice Hamiltonian

$$H_{3D} = -J\sum_r \vec{S}_r \cdot (\vec{S}_{r+a\hat{x}} + \vec{S}_{r+a\hat{y}} + \vec{S}_{r+a\hat{z}}) - K\sum_r (\vec{S}_r \times \vec{S}_{r+a\hat{x}} \cdot \hat{x} + \vec{S}_r \times \vec{S}_{r+a\hat{y}} \cdot \hat{y} + \vec{S}_r \times \vec{S}_{r+a\hat{z}} \cdot \hat{z}) - \vec{H} \cdot \sum_r \vec{S}_r$$

(4)

The r-sites span the $L \times L \times t$ cubic lattice. Ferromagnetic exchange J, Dzyaloshinskii-Moriya anisotropic exchange K, and the Zeeman coupling to the external magnetic field $\vec{H}$ are included in the model. Assuming slowly varying spin configuration results in the continuum model given in the text,

$$H = \int d^3r \left[\frac{(J/a)}{2}(\nabla\vec{M})^2 + (K/a^2)\vec{M} \cdot (\nabla \times \vec{M}) - (\vec{H}/a^3) \cdot \vec{M} \right]. \qquad (5)$$

The lattice Hamiltonian Eq. (4) is regarded as a lattice adaptation of the continuum Hamiltonian Eq. (5), once appropriate identification between the lattice and continuum model parameters is made as $(J/a, K/a^2, \vec{H}/a^3)_{lattice} \rightarrow (J, K, \vec{H})_{continuum}$. The lattice

spacing a is the typical size of the block inside which microscopic spins can be treated as constant.

Simulations were first performed by increasing the layer thickness t from 1 to d - the wavelength of the spiral spin modulation. Up to this thickness the resulting low-temperature spin patterns within each layer are the same as those of a single two-dimensional plane. Thus we can reduce the model to a two-dimensional (2D) one by turning off the irrelevant interaction for the z-direction bonds and treating all the

$$H_{2D} = -J\sum_r \vec{S}_r \cdot (\vec{S}_{r+a\hat{x}} + \vec{S}_{r+a\hat{y}}) - K\sum_r (\vec{S}_r \times \vec{S}_{r+a\hat{x}} \cdot \hat{x} + \vec{S}_r \times \vec{S}_{r+a\hat{y}} \cdot \hat{y}) - \vec{H} \cdot \sum_r \vec{S}_r . \qquad (6)$$

spins sharing the same (x, y) coordinate as a single spin.

The parameters of the 2D model are obtained from those in the 3D model through multiplying by the layer thickness t.

Each classical spin $\vec{S}_r$ in the 2D model is taken to have the unit length, $(\vec{S}_r)^2 = 1$. Periodic boundary conditions were imposed on a $L \times L$ lattice and single-flip Metropolis algorithm was used throughout the calculation. The ratio K / J was chosen to yield the spiral propagation wave vector, $\vec{k} = (k, k)$ with k determined by $\tan(k) = K / \sqrt{2}J$.

Wavelengths of $d = 6$ ($k = 2\pi/6$) lattice constants on 36x36 lattice and $d = 10$ ($k = 2\pi/10$) on 30x30 lattice were used for most of the simulation results. These values of d are large enough for the continuum approximation Eq. (5) to be justified. Magnetic field orientation was fixed along the z-direction, as in the experimental setup. Two independent schemes were employed to check the consistency of the simulation: (1) *Temperature sweep*: At each fixed *K/J* and *H*, temperatures were gradually lowered down to *T/J* = 0.01 during the MC update to reach the correct ground state. (2) *Field*

sweep: At a fixed temperature T, magnetic field strength H was gradually increased from zero to a large enough value to yield a completely ferromagnetic state. Equilibrium situation for a given parameter set was typically reached well within the first 10^5 MC steps, and the next 10^5 MC configurations were used to compute physical quantities such as the Skyrmion number.

Phase diagram shown in Fig. 3 was obtained from the combination of temperature and field sweep MC procedures outlined above. The Skyrmion crystal (S$_k$X) phase boundary was identified from a combination of the inspection of the real-space image of a triangular lattice structure of Skyrmions, the hexagonal Bragg patterns in the Fourier analysis, and a sharp increase/decrease in the calculated Skyrmion number. The phase boundary separating the helical spin (H) phase from the H+S$_k$ region in Fig. 3h is characterized by the appearance of isolated Skyrmions forming defects in the spin stripe structure. The defects increase in density upon increasing the field strength and eventually fill the whole space as a hexagonal array when S$_k$X phase is established. The region intervening S$_k$X and ferromagnetic phase (FM+S$_k$ in Fig. 3h) is characterized by the "thinning out" of the Skyrmions as well as disordering in their positions. At high temperature where the S$_k$X phase is no longer identifiable, the crossover from H+S$_k$ to FM+S$_k$ occurs in a continuous manner.

References

[1] Onose, Y., et al., *Phys. Rev. B* **72**, (2006) 224431.

[2] P. J. Grundy and R. S. Tebble, *Adv. Phys.* **17** (1968) 153.

[3] M.R. Teague, *J. Opt. Soc. Am.* **73** (1983) 1434.

[4] K. Ishizuka and B. Allman, *J. Electron Microsc.* **54** (2005) 191.

[5] S. Bajt, et al., *Uitramicroscopy* **83** (2000) 67.

[6] M. Onoda, et al., J. Phys. Soc. Jpn. **73** (2004) 2624.
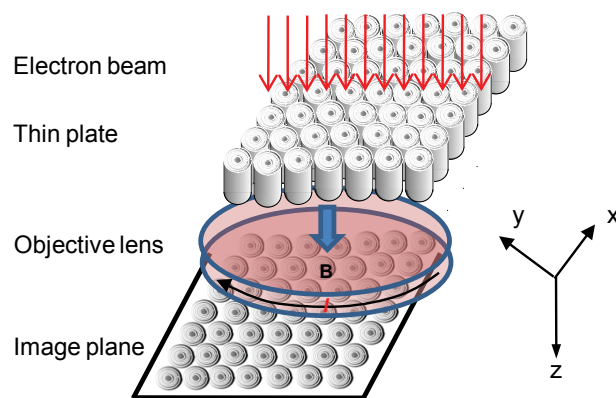
Supplemental Figure 1: Sketch of Lorentz transmission electron microscopy.
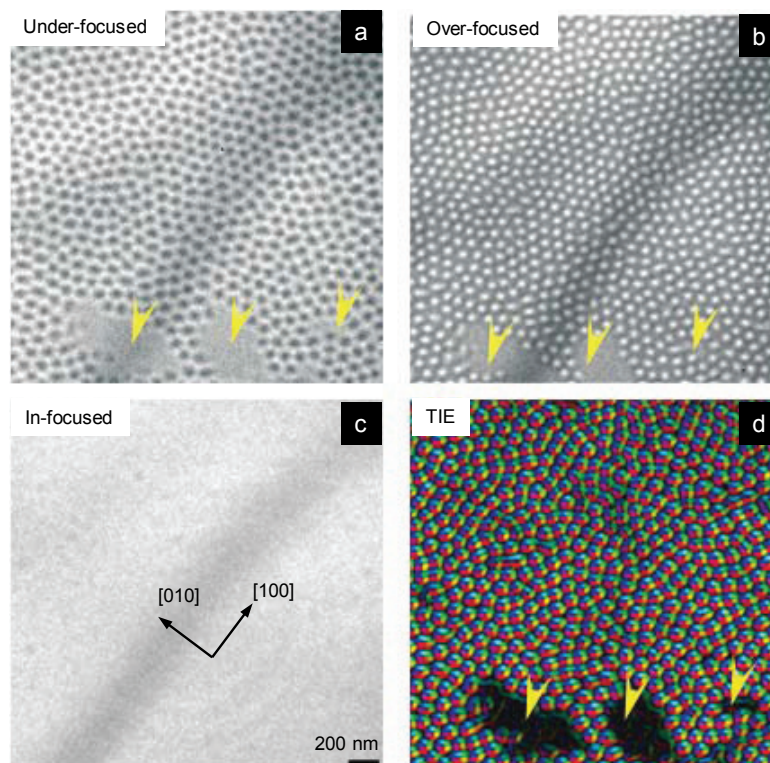
Supplemental Figure 2: Skyrmion crystal structure in $Fe_{0.5}Co_{0.5}Si$ under an external magnetic field of 50 mT normal to the image plane. a-c: The under-, over- and in-focused Lorentz TEM images. d: Transport-of-intensity equation (TIE) image obtained by using the commercial software, QPt, based on such three Lorentz TEM images. The defects of Skyrmion crystal are signed by yellow arrows.
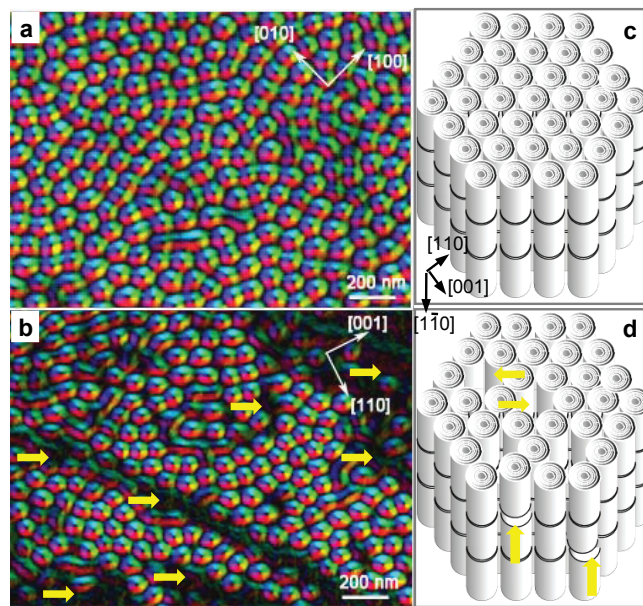
Supplemental Figure 3: Skyrmion crystal structure (a-b) and schematic of hexagonal vortex structure (c-d) in $Fe_{0.5}Co_{0.5}Si$ at 25 K under an applied field of 50 mT. (c) and (d) represent the schematics of ordered and disordered vortex structures, respectively.
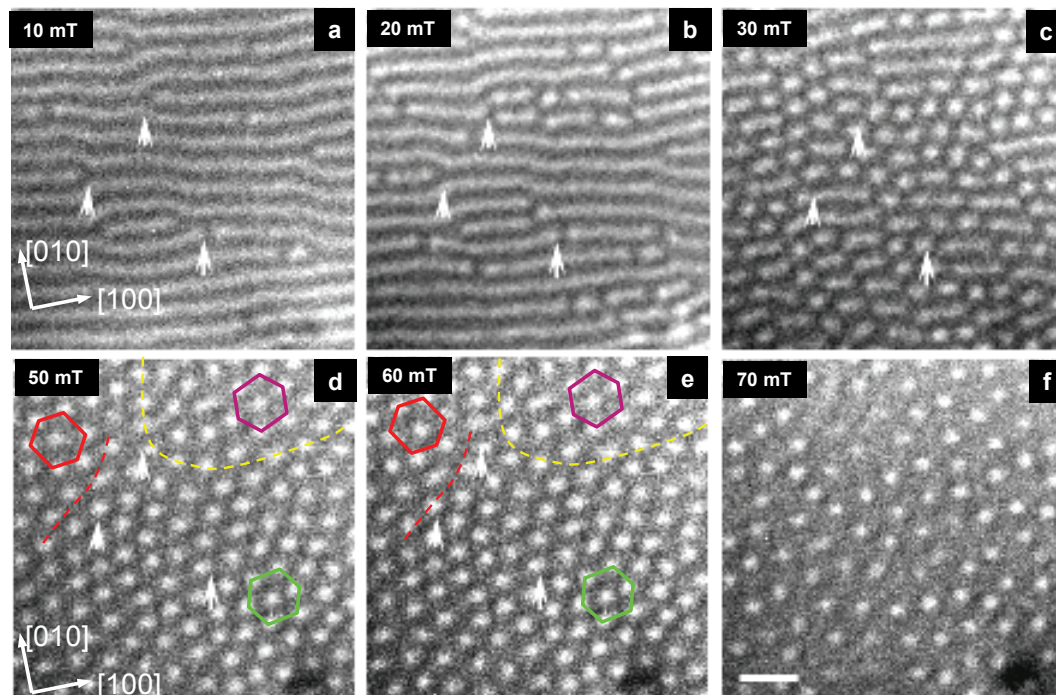
Supplemental Figure 4: Formation of Skyrmion crystal in $Fe_{0.5}Co_{0.5}Si$ under external magnetic fields which were applied along the c-axis. Dislocations of the magnetic structure and the domain boundaries of Skyrmion crystal are shown by white arrows and color dashed lines, respectively.